

Transition of propagation of relativistic particles from the ballistic to the diffusion regime

A. Yu. Prosekin*

Max-Planck-Institut für Kernphysik, Saupfercheckweg 1, D-69117 Heidelberg, Germany

S. R. Kelner

*Max-Planck-Institut für Kernphysik, Saupfercheckweg 1, D-69117 Heidelberg, Germany
and Research Nuclear University (MEPHI), Kashirskoe shosse 31, 115409 Moscow, Russia*

F. A. Aharonian

*Dublin Institute for Advanced Studies, 31 Fitzwilliam Place, Dublin 2, Ireland
and Max-Planck-Institut für Kernphysik, Saupfercheckweg 1,
D-69117 Heidelberg, Germany*

(Received 23 June 2015; published 8 October 2015)

A stationary distribution function that describes the entire process of the propagation of relativistic particles, including the transition between the ballistic and diffusion regimes, is obtained. The spacial component of the constructed function satisfies the first two moments of the Boltzmann equation. The angular part of the distribution provides accurate values for the angular moments derived from the Boltzmann equation, and gives a correct expression in the limit of the small-angle approximation. Using the derived function, we study the gamma-ray images produced through the pp interaction of relativistic particles with gas clouds in the proximity of the accelerator. In general, the morphology and the energy spectra of gamma rays significantly deviate from the “standard” results corresponding to the propagation of relativistic particles strictly in the diffusion regime.

DOI: [10.1103/PhysRevD.92.083003](https://doi.org/10.1103/PhysRevD.92.083003)

PACS numbers: 96.50.sb, 13.85.Tp, 98.70.Sa, 98.70.Rz

I. INTRODUCTION

The propagation of cosmic rays in turbulent magnetic fields can proceed in different regimes depending on the scales under consideration. On small scales, when the particles move coherently, their propagation is ballistic. This usually occurs close to the source, just after the particles escape the sites of their acceleration. With time, the multiple stochastic scattering in turbulent magnetic fields leads to the isotropization of the directions of cosmic rays. The complete isotropization implies that the propagation proceeds in the diffusion regime.

The limiting cases of the small-angle and isotropic particle distributions allow for solutions of the problem of particle propagation on small and large scales, respectively [1–3]. The small-angle approximation fails when the deflection of particles becomes large, typically larger than one radian. The solution of the diffusion equation, in addition to its inability to be applied to small spacial scales, faces the so-called problem of superluminal propagation [4]. In this regard, the apparent requirement $r^2/D \gtrsim r/c$ implies that the diffusion works at distances $r \gtrsim D/c$, where D is the diffusion coefficient and c is the speed of light.

In the small-angle approximation, the evolution of the angular distribution has a diffusive character [1,2]. However, since the pitch angle changes within the limited

interval, $-1 \leq \mu \leq 1$ (μ is the cosine of the pitch angle), the mean square displacement of the pitch angle deviates from diffusive behavior as the average deflection angle grows. For the isotropic turbulence, the moments of the pitch-angle distribution on large time scales have an exponential behavior [5]. This means that the isotropization becomes fast after the characteristic time which is determined by the pitch-angle Fokker-Planck coefficient $D_{\mu\mu}$. On the other hand, a slower isotropization can happen if the turbulent magnetic field has a slab geometry.

In this work we use the method of moments. It allows us to eliminate the angular dependence at the expense of the introduction of an isotropization function that determines the dynamics of isotropization. The final results depend on the form of the isotropization function. However, as we demonstrate below, for a reasonable choice of the form of the function, the results remain quite stable.

To avoid the problem of superluminal motion, Aloisio *et al.* [4] have introduced the so-called Jüttner function, which describes the evolution of the cosmic-ray density. Although this function is obtained phenomenologically from the formal similarity between the diffusion propagator and the Maxwellian distribution, it gives correct results in the limiting cases of diffusion and the ballistic regime. Below we will show that the Jüttner function integrated over time is close to our stationary solution, which proceeds from the Boltzmann equation.

*Anton.Prosekin@mpi-hd.mpg.de

In many cases, especially for the problems related to the radiation of cosmic rays, it is necessary to know not only the cosmic-ray density but also their angular distribution. Indeed, the part of radiation emitted by particles with a strongly anisotropic distribution can have a strong impact on the morphology and spectrum of radiation, or even be simply missed by the observer.

To demonstrate the importance of the angular distribution for the apparent gamma-ray morphology, we calculate the gamma-ray intensity maps of the regions surrounding the cosmic-ray accelerator. The most distinct features can be seen for the clumps of matter close to the source. The anisotropy changes the radiation spectrum significantly and leads to a fast decrease of the intensity at high energies. This results in a suppression or a disappearance of radiation from nearby clouds located away from the line of sight towards the cosmic-ray source. Moreover, even in the case of a homogeneous matter distribution, the effects of anisotropy and the transition from the ballistic to the diffusion regime play an important role in the formation of gamma-ray morphology.

The paper is organized as follows. In Sec. II we describe the formalism based on the Boltzmann equation, and obtain the stationary distribution function, which is valid for all scales from the ballistic to the diffusion regime. In Sec. III, this distribution function is used for calculations of the gamma-ray morphology of nearby clouds irradiated by cosmic rays. The conclusions are summarized in Sec. IV.

II. ANALYTICAL DESCRIPTION

A. Method of moments

Let us consider the evolution of the distribution function in the case of multiple stochastic scatterings. Here we do not specify the mechanism of the scattering, and describe the processes only by the generic probability of the particle to be scattered. The evolution of the distribution function $f(t, \mathbf{r}, \mathbf{n})$ is determined by the Boltzmann transport equation

$$\frac{\partial f}{\partial t} + \mathbf{n} \frac{\partial f}{\partial \mathbf{r}} = Stf + \frac{\delta(t)\delta(\mathbf{r})}{4\pi}, \quad (1)$$

where the speed of the light (propagation speed of ultra-relativistic particles) is set to $c = 1$. Here \mathbf{n} is the unit vector in the direction of propagation. It is assumed that the particles are injected by an instant spherically symmetric point-like source described by the Dirac delta functions $\delta(t)\delta(\mathbf{r})$. We consider only elastic collisions which are described by the collision integral

$$Stf = \int f(\mathbf{n}')w(\mathbf{n}' \rightarrow \mathbf{n})d\Omega' - \int f(\mathbf{n})w(\mathbf{n} \rightarrow \mathbf{n}')d\Omega', \quad (2)$$

where $w(\mathbf{n}' \rightarrow \mathbf{n})$ is the probability of the scattering of a particle from the initial direction along \mathbf{n}' to the final direction along \mathbf{n} per unit time. In the case of an isotropic medium, the probability w depends only on the angle between the initial and final directions. For compactness of presentation, the dependence of the distribution function on time and the coordinates in Eq. (2) is omitted.

The solution of Eq. (1) can be found in the small-angle approximation, which is valid for initial moments of time. Below we will show that from this equation one can also obtain the equation for the diffusion of particles, and derive its solution which is valid for large time intervals.

We are interested, first of all, in the transition between these two solutions. For this purpose it is useful to simplify the problem and consider the moments of the distribution function rather than the distribution function itself. Applying successively the integral operators $\int d\Omega$, $\int d\Omega n_\alpha, \dots, \int d\Omega n_\alpha \dots n_\omega$ to the Boltzmann equation, one can obtain the equations for the moments. We restrict ourselves to the first two moments: the density $g = \int f d\Omega$ and the current $\mathbf{j} = \int \mathbf{n} f d\Omega$. They are governed by the following equations:

$$\begin{aligned} \frac{\partial g}{\partial t} + \frac{\partial j_\alpha}{\partial r_\alpha} &= \delta(t)\delta(\mathbf{r}), \\ \frac{\partial j_\alpha}{\partial t} + \frac{\partial}{\partial r_\beta} \langle n_\alpha n_\beta \rangle g &= -\frac{j_\alpha}{\tau}. \end{aligned} \quad (3)$$

Here τ is the scattering time, which is the inverse of the transport cross section $\sigma_{tr} = 1/\tau$, where

$$\sigma_{tr} = \int (1 - \mathbf{nn}')w(\mathbf{n}' \rightarrow \mathbf{n})d\Omega. \quad (4)$$

In the derivation of the equations in Eq. (3), it has been taken into account that $\int n_\alpha d\Omega = 0$, $\int Stf d\Omega = 0$.

The density and the current depend on the higher moments of the distribution function. To close the system of equations given by Eq. (3), we should define the form of the isotropization tensor,

$$\langle n_\alpha n_\beta \rangle = \frac{\int n_\alpha n_\beta f d\Omega}{\int f d\Omega}, \quad (5)$$

based on the following physical arguments.

In the spherically symmetric case, the radial direction is the only preferential direction; therefore, the isotropization tensor should have the following structure:

$$\langle n_\alpha n_\beta \rangle = A\delta_{\alpha\beta} + B\rho_\alpha\rho_\beta, \quad (6)$$

where $\rho = \mathbf{r}/r$ is the radial direction. The standard procedure for the determination of the coefficients A and B , which consists in the consequent multiplication by tensors $\delta_{\alpha\beta}$ and $\rho_\alpha\rho_\beta$, leads to the equations

$$1 = 3A + B, \quad \langle (\mathbf{n}\rho)^2 \rangle = A + B, \quad (7)$$

from which we find

$$A = \frac{1 - \langle (\mathbf{n}\rho)^2 \rangle}{2}, \quad B = \frac{3\langle (\mathbf{n}\rho)^2 \rangle - 1}{2}. \quad (8)$$

We assume that the tensor depends only on the coordinates. Then, it is convenient to introduce the isotropization function $\phi(r) = B$ which would allow us to write the isotropization tensor in the form

$$\langle n_\alpha n_\beta \rangle = (1 - \phi(r)) \frac{\delta_{\alpha\beta}}{3} + \phi(r) \rho_\alpha \rho_\beta. \quad (9)$$

The tensor consists of the unidirectional ($\rho_\alpha \rho_\beta$) and the isotropic ($\delta_{\alpha\beta}/3$) parts. At $r = 0$, when $\mathbf{n} = \boldsymbol{\rho}$, we have $\langle n_\alpha n_\beta \rangle(0) = \rho_\alpha \rho_\beta$, whereas at the infinity all directions of \mathbf{n} are distributed isotropically, and $\langle n_\alpha n_\beta \rangle(\infty) = \delta_{\alpha\beta}/3$. Thus, the isotropization function should satisfy the boundary conditions

$$\phi(0) = 1 \quad \text{and} \quad \phi(\infty) = 0. \quad (10)$$

In the spherically symmetric case, the density and the current are expressed as $g = g(t, r)$ and $\mathbf{j} = j(t, r)\boldsymbol{\rho}$. Then the substitution of the isotropization tensor in the form given by Eq. (9) into Eq. (3) results in

$$\begin{aligned} \frac{\partial G}{\partial t} + \frac{\partial J}{\partial r} &= \frac{\delta(t)\delta(r)}{4\pi}, \\ \frac{\partial J}{\partial t} + \frac{\partial G}{\partial r} - \frac{1}{r} \frac{\partial}{\partial r} \left(\frac{2}{3} (1 - \phi) r G \right) &= -\frac{J}{\tau}, \end{aligned} \quad (11)$$

where we have introduced the new functions $G = r^2 g$ and $J = r^2 j$.

At small distances and times, the current changes fast, i.e., $\frac{\partial J}{\partial t} \gg \frac{J}{\tau}$. Therefore one can neglect the term on the right-hand side of the second equation in Eq. (11). The condition $\phi(0) = 1$ leads to the cancellation of the third term on the left-hand side of the same equation. Thus, the equations in Eq. (11) are reduced to

$$\begin{aligned} \frac{\partial G}{\partial t} + \frac{\partial J}{\partial r} &= \frac{\delta(t)\delta(r)}{4\pi}, \\ \frac{\partial J}{\partial t} + \frac{\partial G}{\partial r} &= 0, \end{aligned} \quad (12)$$

which can be rewritten in the form of the wave equation for G ,

$$\frac{\partial^2 G}{\partial t^2} = \frac{\partial^2 G}{\partial r^2}, \quad (13)$$

with the boundary condition $G(t = +0, r) = \delta(r)/4\pi$. The solution of this equation in terms of the density $g = G/r^2$ is

$$g(t, r) = \frac{1}{4\pi r^2} \delta(r - t), \quad (14)$$

which describes the behavior of the density in the ballistic regime.

In the opposite case, i.e., for large distances and times, it is more convenient to proceed from the initial system of equations given by Eq. (3). The current changes slowly on the scale of the scattering time τ , i.e., $\frac{\partial j}{\partial t} \gg \frac{j}{\tau}$. This allows us to neglect the derivative $\frac{\partial j}{\partial t}$ in the second equation. Taking into account that $\phi = 0$, we find

$$\begin{aligned} \frac{\partial g}{\partial t} &= -\nabla \mathbf{j}, \\ \mathbf{j} &= -\frac{\tau}{3} \nabla g, \end{aligned} \quad (15)$$

which can be rewritten in the form of the diffusion equation for g ,

$$\frac{\partial g}{\partial t} = \frac{\tau}{3} \Delta g. \quad (16)$$

A comparison with the conventional form of the diffusion equation gives the well-known relation

$$D = \frac{c^2 \tau}{3} = \frac{c l_c}{3}, \quad (17)$$

where $l_c = c\tau$ is the scattering length.

B. Stationary case

The system of equations derived in the previous section describes the particle motion over the entire process of propagation, including the ballistic and diffusion modes, as well as the transition stage between these two regimes. It has a simple stationary solution. Indeed, the integration over the entire time cancels out the time derivatives and leads to the following system of ordinary differential equations:

$$\begin{aligned} \frac{dJ}{dr} &= \frac{\delta(r)}{4\pi}, \\ \frac{dG}{dr} - \frac{1}{r} \frac{d}{dr} \left(\frac{2}{3} (1 - \phi) r G \right) &= -\frac{J}{\tau}, \end{aligned} \quad (18)$$

where $J = J(r)$ and $G = G(r)$. The first of these equations gives $J = \Theta(r)/4\pi$, where $\Theta(r)$ is the Heaviside step function. The substitution of the current J into the second equation results in an ordinary differential equation of the first order. Its solution can be presented in the form

$$g(r) = \frac{\chi(r)}{4\pi r^2 \tau} \int_r^\infty dr' \exp\left(-\int_r^{r'} \psi(r'') dr''\right), \quad (19)$$

where

$$\chi(r) = \frac{3}{1+2\phi(r)}, \quad \psi(r) = \frac{2}{r} \left(\frac{1-\phi(r)}{1+2\phi(r)} \right). \quad (20)$$

The limits for the integrals are chosen from the condition that the density vanishes at infinity.

To find the final expression, one should choose a suitable form of the isotropization function $\phi(r)$. The boundary condition $4\pi g(r)r^2 \rightarrow 1$ at $r \rightarrow 0$, which has not been used yet, gives a relation between $\phi(r)$ and τ . To take this relation into account, ϕ should have one free parameter ν . In the case of an isotropic medium, one expects an exponential rate of isotropization [5]. Therefore, one of the possible expressions for the isotropization function is

$$\phi(r) = e^{-r/\nu}. \quad (21)$$

However, this function does not allow for a representation of Eq. (19) in quadratures. Another expression,

$$\phi = \frac{1}{1+r/\nu}, \quad (22)$$

is less physically motivated, but it allows us to obtain a simple analytical solution. Indeed, the substitution of Eq. (22) into Eq. (19) results in

$$g(r) = \frac{1}{4\pi r^2} \frac{3(\nu+r)}{\tau}. \quad (23)$$

The boundary condition $4\pi g(r)r^2 \rightarrow 1$ at $r \rightarrow 0$ gives $\nu = \tau/3$. A comparison with Eq. (17) gives $\nu = D/c$. Then, the solution can be written in terms of the diffusion coefficient D as

$$g(r) = \frac{1}{4\pi} \left(\frac{1}{r^2} + \frac{c}{rD} \right), \quad (24)$$

which is just the sum of the solutions in the limiting cases of the ballistic and diffusion regimes. Introducing a dimensionless parameter $x = rc/D$, which is the radial distance in units of D/c , one can rewrite this expression in the form

$$g(r) = \frac{(1+x)}{4\pi r^2}. \quad (25)$$

The result is surprisingly simple. However, we should note that it is obtained for a specific form of the isotropization function. The results for other forms of the isotropization function can be numerically calculated using Eq. (19). Figure 1 shows that the densities obtained for

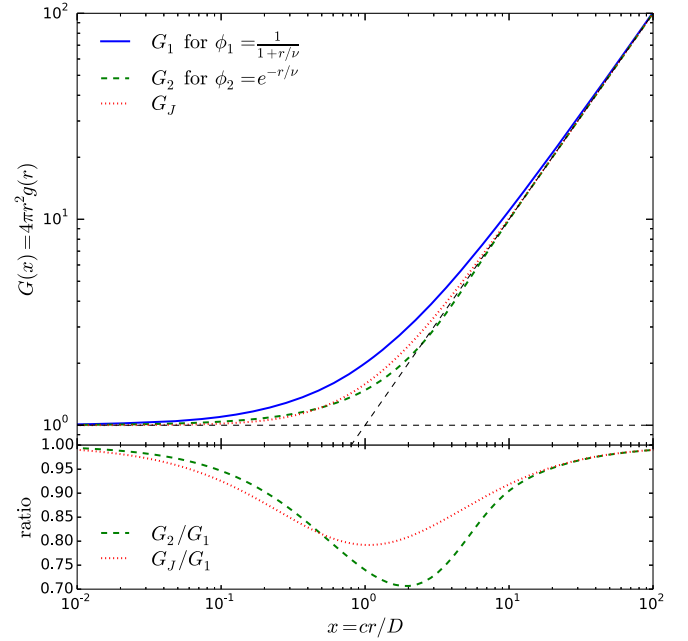


FIG. 1 (color online). Upper panel: The function $G = 4\pi r^2 g(r)$ for different models of isotropization as a function of $x = cr/D$. $G_1(x)$ and $G_2(x)$ correspond to the $\phi_1 = \frac{1}{1+r/\nu}$ and $\phi_2 = e^{-r/\nu}$ isotropization functions. $G_J(x)$ corresponds to the generalized Jüttner function integrated over time proposed in Ref. [4]. The dashed lines represent the asymptotes $G(x) = 1$ and $G(x) = x$. Lower panel: The ratios of the functions: G_2/G_1 and G_J/G_1 .

$\phi = \frac{1}{1+r/\nu}$ and $\phi(r) = e^{-r/\nu}$ differ by less than 30% at $x \sim 1$, and by less than 10% at $x < 0.1$ and $x > 10$. For comparison, we also present the density obtained from the generalized Jüttner function integrated over time. This function was proposed phenomenologically in Ref. [4] as a description of the evolution of the cosmic-ray flux. It is seen from Fig. 1 that the Jüttner function gives a result which is quite close to the solution with an exponential form of the isotropization function.

The propagation of cosmic rays is characterized not only by the density, but also by the angular distribution of the particles. Such information is contained in the moments of the angular distribution. Indeed, if $\mu = \mathbf{n}\boldsymbol{\rho}$ is the cosine of the angle between the particle and the radial direction, then the first moment of the angular distribution is

$$\langle \mu \rangle = \frac{\mathbf{j}\boldsymbol{\rho}}{g}. \quad (26)$$

Using the solution given by Eq. (25), we have

$$\langle \mu \rangle = \frac{1}{1+x}. \quad (27)$$

The second moment is just the projection of the isotropization tensor on the radial direction,

$$\langle \mu^2 \rangle = \langle n_\alpha n_\beta \rangle \rho_\alpha \rho_\beta = \frac{1 + 2\phi(r)}{3}. \quad (28)$$

The moments $\langle \mu \rangle$ and $\langle \mu^2 \rangle$ can be used to construct a function that has the properties of the exact angular distribution. In this regard, the simplest function is

$$M(\mu) = \frac{1}{Z} \exp\left(-\frac{3(1-\mu)}{x}\right), \quad (29)$$

where the normalization function has the form

$$Z(x) = \frac{x}{3}(1 - e^{-6/x}). \quad (30)$$

$M(\mu)$ is the distribution of the cosine of the pitch angles μ in the interval $[-1, 1]$. This distribution provides moments that are in a good agreement with the moments given by Eqs. (27) and (28). This can be seen in Fig. 2, which shows the first moment obtained from Eq. (26) for different isotropization functions and the first moment of the distribution $M(\mu)$. Moreover, for comparison we show the function

$$\langle \mu \rangle_4 = \frac{1}{x}(1 - e^{-x - \frac{7}{18}x^2}) \quad (31)$$

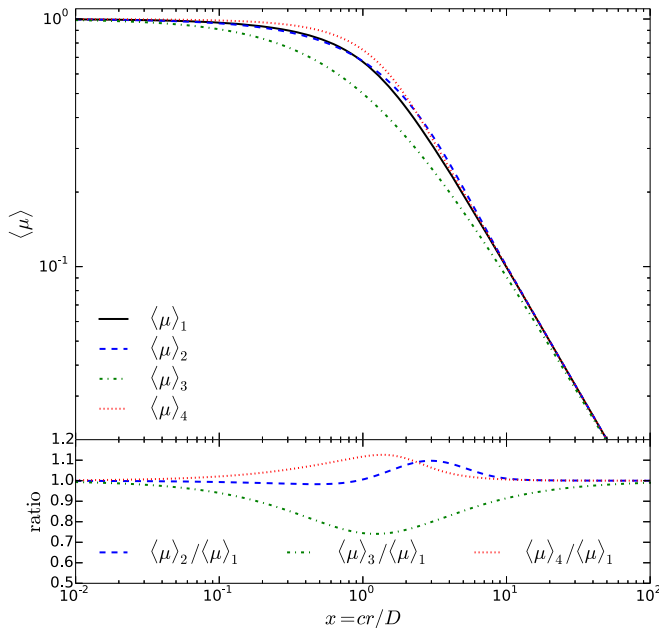


FIG. 2 (color online). Upper panel: The first moment of the angular distribution $\langle \mu \rangle$ for different models of isotropization as a function of $x = cr/D$. $\langle \mu \rangle_2$ and $\langle \mu \rangle_3$ correspond to the $\phi_2 = e^{-r/\nu}$ and $\phi_1 = \frac{1}{1+r/\nu}$ isotropization functions, respectively. $\langle \mu \rangle_1$ is the first moment of the angular distribution $M(\mu)$ given by Eq. (29). $\langle \mu \rangle_4$ is the fit of the numerical results obtained in Ref. [6] given by Eq. (31). Lower panel: The ratios of the functions: $\langle \mu \rangle_2 / \langle \mu \rangle_1$, $\langle \mu \rangle_3 / \langle \mu \rangle_1$, and $\langle \mu \rangle_4 / \langle \mu \rangle_1$.

obtained in Ref. [6] as a fit to the numerical results for the propagation of cosmic rays in turbulent magnetic fields (see Eq. (21) in Ref. [6]). It is seen that all results do not differ by more than 30%. The first angular moment for the isotropization function $\phi(r) = e^{-r/\nu}$ and the moment given by Eq. (31) are within 10% from the first moment of $M(\mu)$.

One can show that in the small-angle limit the distribution given by Eq. (29) describes the diffusion in angle. Indeed, in this limit the transport cross section becomes

$$\begin{aligned} \sigma_{tr} &\approx \int \left(1 - \left(1 - \frac{\theta^2}{2}\right)\right) w(\mathbf{n}' \rightarrow \mathbf{n}) d\Omega \\ &= \frac{1}{2} \left\langle \frac{\Delta\theta^2}{\Delta t} \right\rangle = \frac{D_\theta}{2}, \end{aligned} \quad (32)$$

where D_θ is the diffusion coefficient in angular space. Taking into account Eq. (17) and the relation $x = rc/D$, we obtain

$$M(\mu) \sim \exp\left(-\frac{3D(\theta^2/2)}{rc}\right) = \exp\left(-\frac{\theta^2}{D_\theta r/c}\right). \quad (33)$$

The combination of the density and the angular distributions results in the stationary distribution function

$$f(r, \mu) = \frac{Q}{4\pi c} \left(\frac{1}{r^2} + \frac{c}{rD}\right) \frac{1}{2\pi Z} \exp\left(-\frac{3D(1-\mu)}{rc}\right), \quad (34)$$

which describes the evolution of propagation from the ballistic to the diffusion regime, where Q is the source function (the production rate) of cosmic rays in the source.

We would like to emphasize once more that the exact analytical distribution function is unknown. However, the different models of isotropization produce very similar results. Therefore, the obtained distribution function can be considered as a good (within 30%) approximation to the actual distribution.

C. Diffusion coefficient

In the derived distribution functions the diffusion coefficient is assumed to be constant in space, but it can have an arbitrary energy dependence. The latter is determined by the relation between the Larmor radius $R_L = E/eB$ and the correlation length of the turbulence λ . If $R_L \gg \lambda$, the particle is only slightly deflected on the correlation length. The random walk of uncorrelated deflections results in the scattering length $l_c \sim R_L^2$ [7]. By combining Eq. (17), Eq. (32), and the relation $\tau = 1/\sigma_{tr}$, we obtain

$$D = \frac{2}{3} \frac{c^2}{D_\theta}. \quad (35)$$

The coefficient of diffusion in the angle, D_θ , can be written as [2]

$$D_\theta = \frac{(\alpha - 1)(\beta + 1)}{4\alpha\beta} \frac{c\lambda}{R_L^2}, \quad (36)$$

where α and β are the power-law indices of turbulence for wave vectors $k > k_0 = 2\pi/\lambda$ and $k < k_0$, respectively. The value of β is poorly known; here, we will assume $\beta = 1$.

For the Kolmogorov spectrum of turbulence ($\alpha = 5/3$), calculations of the diffusion coefficient in the regime $R_L \gg \lambda$ give

$$D = \frac{10}{3} c\lambda \left(\frac{R_L}{\lambda}\right)^2. \quad (37)$$

Note that the energy dependence in this regime is the same for any other spectrum of turbulence.

At $R_L \ll \lambda$, particles are only scattered by magneto-hydrodynamic waves with a length equal to their gyroradius. This leads to the dependence of the diffusion coefficient on the turbulence spectrum. The quasilinear theory predicts $l_c \sim R_L^{2-\alpha}$ [8], where α is the power-law index of the turbulence spectrum. This dependence can be obtained as follows. The scattering frequency of the particle by waves is expressed as [9]

$$\nu_s = \frac{\pi}{4} \Omega \left(\frac{\mathcal{E}_k k}{B^2/8\pi} \right)_{|k=k_{\text{res}}}, \quad (38)$$

where \mathcal{E}_k is the spectrum of turbulence normalized as $\int \mathcal{E}_k dk = B^2/8\pi$, $k_{\text{res}} = \Omega/\nu\mu$ is the resonance wave vector, Ω is the gyrofrequency, and μ is the cosine of the pitch angle. The diffusion coefficient is related to the scattering frequency as [7,8]

$$D = \frac{v^2}{4} \int_0^1 d\mu \frac{1-\mu^2}{\nu_s}. \quad (39)$$

Taking the turbulence spectrum in the form $\mathcal{E}_k \sim 1/k^\alpha$ with the minimum wave vector $k_0 = 2\pi/\lambda$, and substituting Eq. (38) into Eq. (39), we obtain

$$D = \frac{2}{(2-\alpha)(4-\alpha)(\alpha-1)} \frac{1}{\pi(2\pi)^{\alpha-1}} \lambda c \left(\frac{R_L}{\lambda}\right)^{2-\alpha}. \quad (40)$$

Thus, for $\alpha = 5/3$ we have

$$D = \frac{27}{7} \frac{1}{\pi(2\pi)^{2/3}} \lambda c \left(\frac{R_L}{\lambda}\right)^{1/3}, \quad R_L \ll \lambda. \quad (41)$$

We note that the values of the numerical prefactors in Eqs. (37) and (41) depend slightly on the turbulence spectrum. The parameter λ in these expressions corresponds to the largest scale of the inertial range of turbulence and can be associated with the correlation length.

The simulations of particle propagation in the isotropic and purely turbulent magnetic field performed in Ref. [10]

show that the diffusion coefficient can be presented in the form

$$D = \frac{c\lambda}{3} \left(\frac{1}{(2\pi)^{2/3}} \left(\frac{R_L}{\lambda}\right)^{1/3} + \frac{4\pi}{3} \left(\frac{R_L}{\lambda}\right)^2 \right). \quad (42)$$

In the next section, this convenient expression for the diffusion coefficient will be used for calculations of the gamma-ray emission.

III. GAMMA-RAY EMISSION OF THE REGION SURROUNDING A COSMIC-RAY ACCELERATOR

High-energy gamma rays not only carry unique information about the accelerators of cosmic rays (electrons, protons, and nuclei), but they also allow us to trace these particles after they leave the sites of their acceleration. In the interstellar medium, this is realized through interactions of cosmic rays with the so-called giant molecular clouds. These dense gas regions illuminated by cosmic rays provide a target for proton-proton interaction and radiate gamma rays. Thus they can serve as unique ‘‘barometers’’ for measurements of the pressure (energy density) of cosmic rays at different locations relative to the accelerator.

The massive clouds located in the vicinity of the accelerator dramatically increase the chances of tracing the runaway particles through the secondary gamma rays. For example, for a young supernova remnant (as an accelerator of cosmic rays) at a distance of 1 kpc, a gas cloud with a mass of order of $10^4 M_\odot$ can emit very high-energy gamma rays at a level detectable by current instruments if the cloud is located within 100 pc of the supernova remnant [11]. Before being fully diffused and integrated into the ‘‘sea’’ of Galactic cosmic rays, they produce gamma rays with a spectrum that could essentially differ from both the gamma-ray spectrum of the accelerator itself and the spectrum of the diffuse Galactic gamma-ray emission. In the case of propagation in a ‘‘nominal’’ diffusion regime, the formation of gamma-ray energy spectra has been discussed in Ref. [12]. However, closer to the accelerator, the propagation of cosmic rays may have a more complex character, which would be reflected in the spectra of secondary gamma rays.

The morphology of the gamma-ray emission is determined by the interplay between the cosmic-ray and matter distributions. While the distribution of the matter could be arbitrary and random, the density of the cosmic rays decreases with distance from the accelerator, which means the most intensive radiation should arrive from the dense regions located close to the accelerator.

However, the angular distribution of cosmic rays may lead to a significant deviation from such a simple picture [13]. Indeed, due to the relativistic character of proton-proton interactions, gamma rays are emitted along the direction of the momentum of the incident proton. This

implies that only the protons directed towards the observer give a contribution to the detectable gamma-ray flux. Close to the accelerator, the angular distribution of cosmic rays, which propagate ballistically along the radial direction, is strictly anisotropic. Thus the gamma radiation can arrive from the direction towards the accelerator only in the presence of a significant amount of gas along the line of sight. For the same reason, the nearby clouds not located on the line of sight could be invisible because their radiation is not directed towards the observer. As the distribution of cosmic rays becomes more isotropic, the apparent intensity of the radiation increases with the distance from the accelerator.

On the other hand, if a gas cloud on the line of sight is located sufficiently close to the accelerator, we could see a bright source which would coincide with the accelerator. This can be misinterpreted as a prolific production of gamma rays inside the accelerator, although in reality the accelerator could be a very inefficient gamma-ray emitter.

Thus, the consideration of a transition from the ballistic to the diffusion regime may result in two consequences related to the density and angular distributions of cosmic rays. The first one is the lack of radiation from regions close to the accelerator even in the presence of massive nearby clouds (but located away from the line of sight). On the contrary, we may detect a very bright and focused gamma-ray image if a dense cloud in the proximity of the accelerator appears on the line of sight.

In the following calculations we consider a proton accelerator of power $L_{\text{cr}} = 10^{37}$ erg/s located at a distance $d = 1$ kpc from the observer. The energy spectrum of protons is taken in the form $J_{\text{cr}}(E) = E^{-2} \exp(-E/10^{15} \text{ eV})$. The stationary distribution of cosmic rays around the accelerator is described by Eq. (34) with the diffusion coefficient given by Eq. (42). We assume that particles

propagate through a turbulent magnetic field with the Kolmogorov spectrum of turbulence. We keep the coherence length of turbulence λ as a free parameter.

In the calculations, the magnetic field is taken at the level of $B = 10^{-4}$ G. In the Galactic disk, the typical value of the diffusion coefficient is $D \approx 10^{28}$ cm²/s at 1 GeV [14]. To match this value we assume $\lambda = 10^4$ pc and $\lambda = 10^5$ pc for the diffusion coefficients, which below we refer to as small and large, respectively. The smallness of the ratio $R_L/\lambda \approx 1.1 \times 10^{-9} E_{12} \lambda_4^{-1}$ (where $E_{12} = E/10^{12}$ eV is the cosmic-ray energy and $\lambda_4 = \lambda/10^4$ pc) allows us to neglect the high-energy nonresonant part of the diffusion coefficient. The estimate based on Eq. (42) gives $D \approx 9 \times 10^{28} E_{12}^{1/3} \lambda_4^{2/3}$ cm²/s. Correspondingly, the transition from the ballistic to the diffusion regime occurs at a characteristic distance $D/c \approx 1.0 E_{12}^{1/3} \lambda_4^{2/3}$ pc from the cosmic-ray source.

Below we consider two cases: (i) a homogeneous massive cloud surrounding the accelerator, and (ii) a group of clouds located near the accelerator. We consider different densities of the background gas (between the clouds), and different values of the diffusion coefficient of cosmic rays. For the calculation of gamma-ray production in pp collisions the parametrization of Ref. [15] has been used. The results present the intensity of gamma radiation integrated along the line of sight through the gamma-ray production region.

In the first example, we consider a homogeneous cloud with a radius $R = 10$ pc and density $n_p = 100$ cm⁻³. With these parameters the mass of the cloud is $M_{\text{cl}} \approx 10^4 M_{\odot}$. The accelerator is placed in the center of the cloud. The intensity maps of gamma rays at three different energies, $E = 10^{10}$, $E = 10^{11}$, and $E = 10^{12}$ eV, are shown in Fig. 3. The calculations are performed for the case of slow

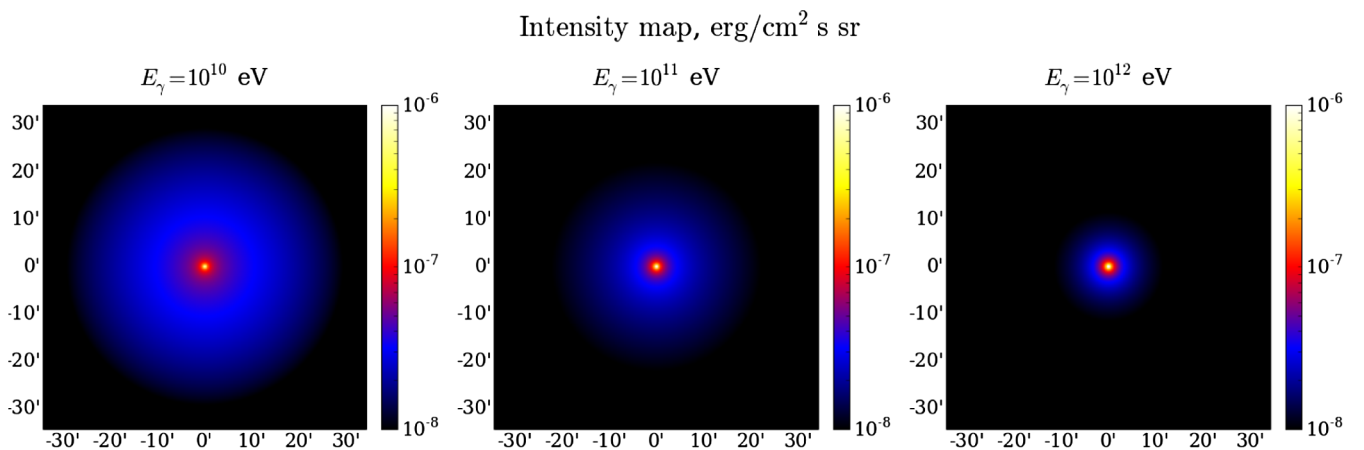


FIG. 3 (color online). The intensity maps of gamma-ray emission at different energies. The spherical cloud with a homogeneous density distribution is irradiated by the cosmic-ray source located at its center. The gas density inside the accelerator is assumed to be very low, so the contribution of the accelerator to the gamma-ray emission is negligible. The maps are produced for the case of a small diffusion coefficient (for details, see the text). For a distance to the source $d = 1$ kpc, the region of $\sim 1^\circ \times 1^\circ$ corresponds to an area $\sim 20 \times 20$ pc².

diffusion. It is assumed that the density inside the accelerator is very small, and thus the gamma radiation of the accelerator itself can be ignored.

Figure 3 shows that with an increase of energy the radiation becomes more concentrated at the position of the accelerator. The change of the gamma-ray morphology is explained by the energy dependence of the cosmic-ray propagation. With an increase of energy, the transition from the ballistic to the diffusion regime occurs at larger distances from the accelerator. The faster decrease of the cosmic-ray density in the ballistic regime results in a faster decrease of gamma-ray intensity at high energies. This is seen in Fig. 4, in which the radial profiles of the intensity at different energies are shown. The left and right panels of Fig. 4 present the results calculated for the small and large diffusion coefficients, respectively. For the fast diffusion, the transition from the steep to the flat part of the profile occurs at larger distances from the accelerator.

In Fig. 4 we show the radial profiles of gamma-ray intensities for two different regimes of diffusion. To describe the behavior of these curves, we also show the local power-law indices $\alpha = d \ln P(r) / d \ln(r)$ at different energies. One can see that at small distances all profiles approach the same inclination with $\alpha \approx -1.3$. At small energies the flat part starts earlier and the intensity decreases more slowly. For example, at $E = 10^9$ eV the flattest part of the profile corresponds to $\alpha \approx -0.3$. With an increase of energy, the flat part becomes steeper. At very

high energies the transition to the flat part might not happen at all.

The angular distribution of cosmic rays has a strong impact on the characteristics of the secondary gamma radiation, in particular on the radial profile of the gamma-ray intensity (see the Appendix). In the case of a strictly radial distribution of particles (i.e., for the ballistic regime of propagation), the gamma-ray source will be detected as a point-like object, independent of the linear size of the gamma-ray production region, L . For the “nominal” diffusion regime, the angular size of the gamma-ray source is determined by the ratio L/R . The transition regime introduces non-negligible corrections to the formation of the overall image of the gamma-ray source, and therefore it should be treated thoroughly. A comparison of the results in Fig. 4 and Fig. 14 (which does not take into account the angular distribution of protons) shows that, in general, the shapes of the radial profiles in these figures are similar, but there is also a significant difference. In particular, if one assumes that the angular distribution of particles is isotropic just after their escape from the source, the power-law index of the slope of the (projected) gamma-ray profile would be $\alpha = -1$. This is in contrast to $\alpha \approx -1.3$, which is expected if we correctly treat the angular distribution of particles closer to the source. The sharp angular distribution of cosmic rays close to the accelerator leads to a considerable loss of emission, and therefore to a steeper gamma-ray intensity profile.

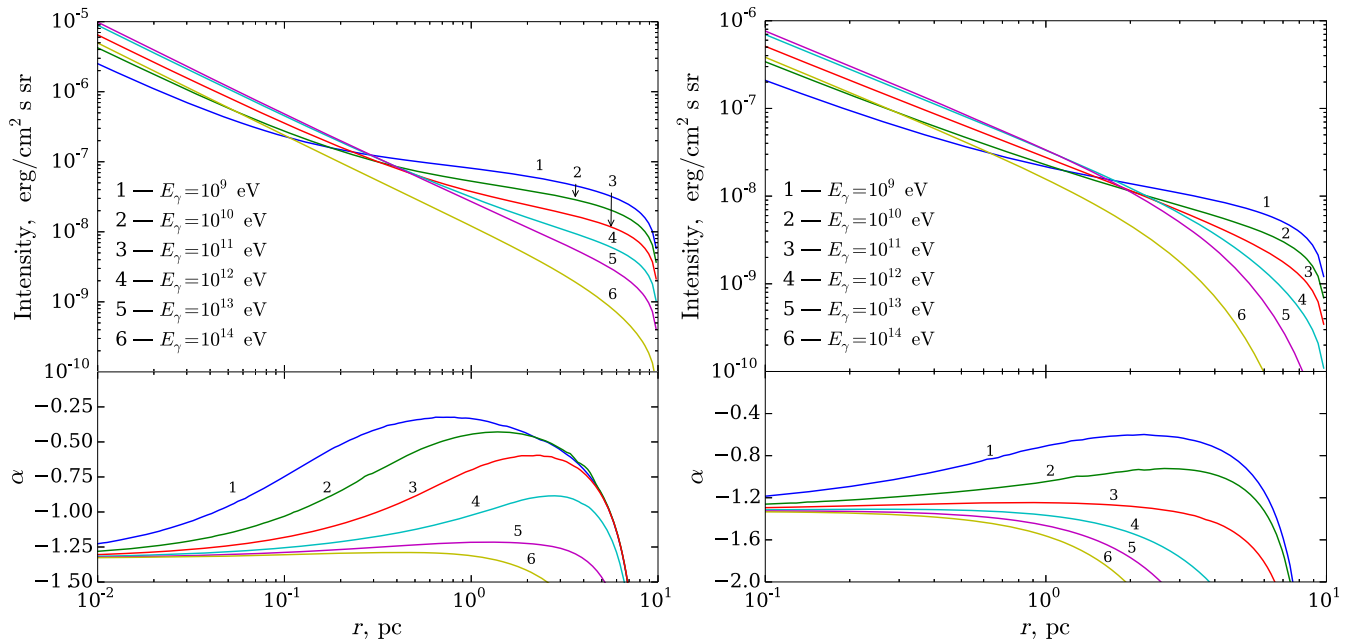


FIG. 4 (color online). Upper panel: Radial intensity profiles for different energies of gamma rays in the case of a homogeneous cloud surrounding the cloud. Lower panel: The power-law index of the respective intensity profiles in the upper panel. The left and right panels present the results calculated for the case of small and large diffusion coefficients, respectively. The profiles for energies $E = 10^{10}$, $E = 10^{11}$, and $E = 10^{12}$ eV in the left panel correspond to the intensity maps shown in Fig. 3.

The spectral energy distributions (SEDs) of gamma rays at different distances from the source of cosmic rays are shown in Fig. 5. The left and right panels show the results corresponding to the small and large diffusion coefficients, respectively. It is seen that an increase of the diffusion coefficient leads to harder gamma-ray spectra. In the case of a homogeneous distribution of the cosmic-ray density and for the power-law energy spectrum of protons with an index $\alpha = 2$, gamma rays have an almost flat SED. Note that the flat part slightly deviates from the cosmic-ray spectrum, namely it contains an intrinsic hardening due to the increase of the inelastic cross section [16]. For the homogeneous distribution of cosmic rays, the flat part of the gamma-ray spectrum can be approximated by a power law with a photon index $\Gamma = 1.94$. The SED in the direction towards the accelerator becomes even harder, with a power-law photon index $\Gamma = 1.86$. This can be explained by the fact that high-energy protons preserve their radial direction longer and, consequently, produce higher-energy radiation towards the observer.

Because of the diffusion of cosmic rays, in directions far from the direction towards the accelerator the density of the low-energy protons decreases more slowly. At large distances from the accelerator, the SED of gamma rays is close to $E^{-\delta}$ (slightly harder because of the pp interaction cross section), where δ characterizes the energy dependence of the diffusion coefficient, $D(E) = D_0 E^\delta$. Because of the assumed dependence of the diffusion coefficient with $\delta = 1/3$, the SED at large distances in Fig. 5 follows a $\propto E^{-1/3}$ dependence.

In more realistic scenarios, the surroundings of the cosmic-ray source could be inhomogeneous, i.e., they may consist of clumps of matter. To study the general features of the radiation of such an environment, we use a simplified gas distribution template consisting of four

identical equally separated clouds surrounded by a homogeneous low-density gas (background):

$$n_p = n_{p0} \left(\sum_i e^{-\left(\frac{r-r_i}{w_i}\right)^2} + x_{\text{bg}} \right), \quad (43)$$

where $n_{p0} = 10^3 \text{ cm}^{-3}$, r_i and w_i are the coordinates of the centers of these clouds and their widths, respectively, and x_{bg} is the level of the background relative to the maximum density in the centers of the clouds. The width of each cloud is $w_i = 1 \text{ pc}$ which corresponds to a mass $M_{\text{cl}} \approx 140 M_\odot$. The separation between the clouds is 5 pc. We consider the cases without the background and with the background with $x_{\text{bg}} = 10^{-2}$. The zero level of the background eliminates the radiation from the direction towards the accelerator. For illustrative purposes, the source of cosmic rays is located at the left border of each map in Fig. 6 and Fig. 7. It is assumed that the density inside the accelerator is very low, and thus its own gamma radiation can be neglected.

The intensity maps for the case without background gas calculated for the slow and fast diffusion of cosmic rays are shown in Figs. 6 and 7, respectively. The corresponding intensity profiles are presented in the left and right panels of Fig. 8. For slow diffusion, the gamma-ray intensity of clouds decreases with the distance from the proton accelerator. The clouds are located along the line perpendicular to the line of sight. At high energies in the case of fast diffusion a fraction of the radiation from the closest clouds is “lost.” Therefore, one can see an interesting effect when—despite the decrease of the cosmic ray density with distance—the highest-energy gamma rays are seen from the farthest rather than the closest clouds.

The results corresponding to the homogeneous gas background are shown in Figs. 9 and 10. The intensity profiles shown in Fig. 11 are smoother compared to the

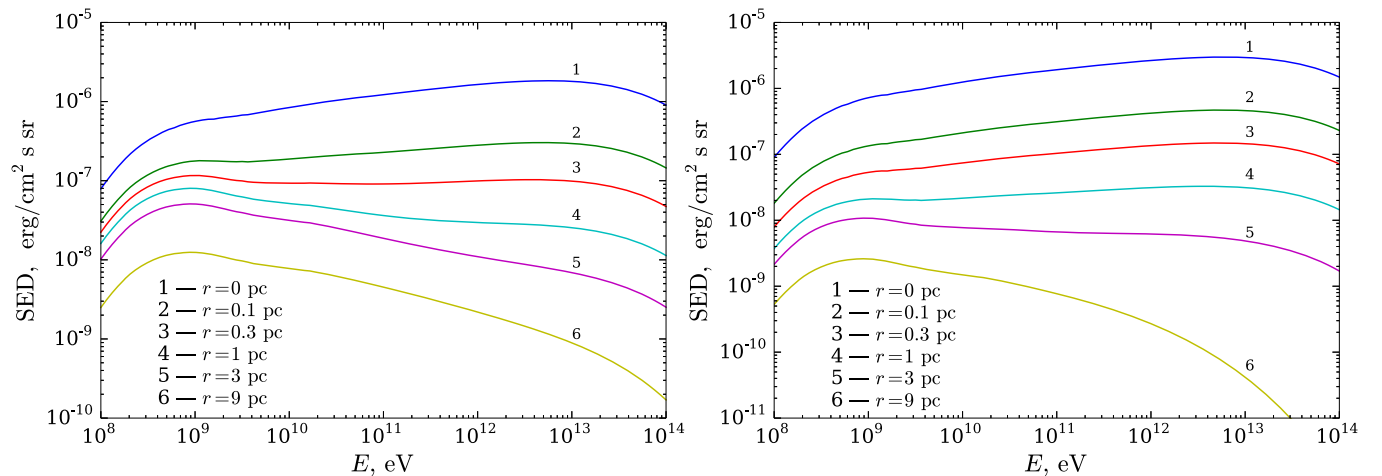


FIG. 5 (color online). Energy spectra of gamma rays at different distances from the cosmic-ray source in the case of a homogeneous cloud. The results are given for the scenarios with slow (left panel) and fast (right panel) proton diffusion.

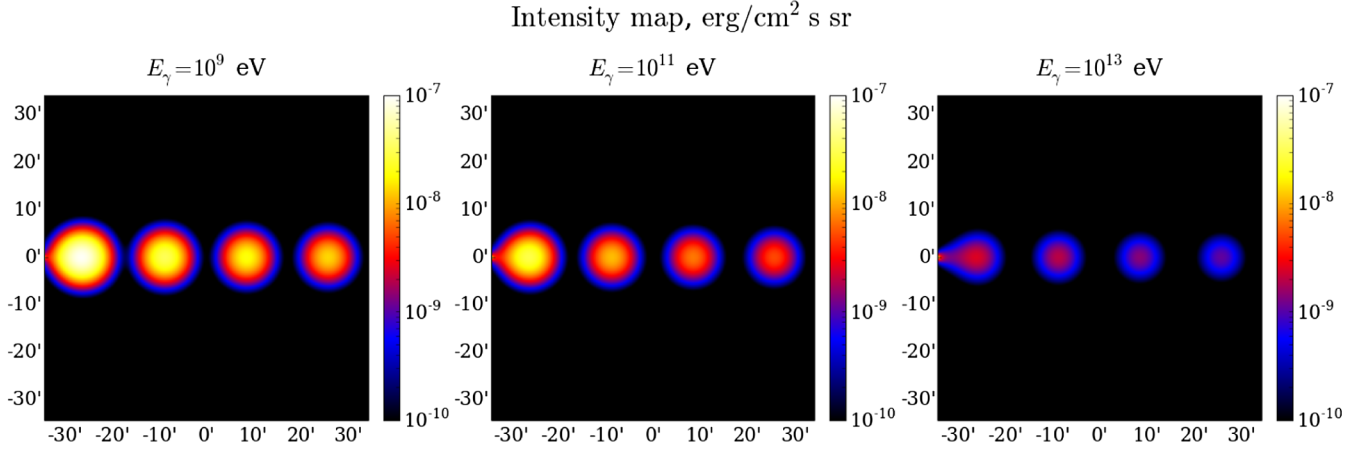


FIG. 6 (color online). The intensity maps of gamma-ray emission from the group of clouds (without the gas background) at various energies for the case of a low diffusion coefficient. The cosmic-ray source is located at the center of the left side.

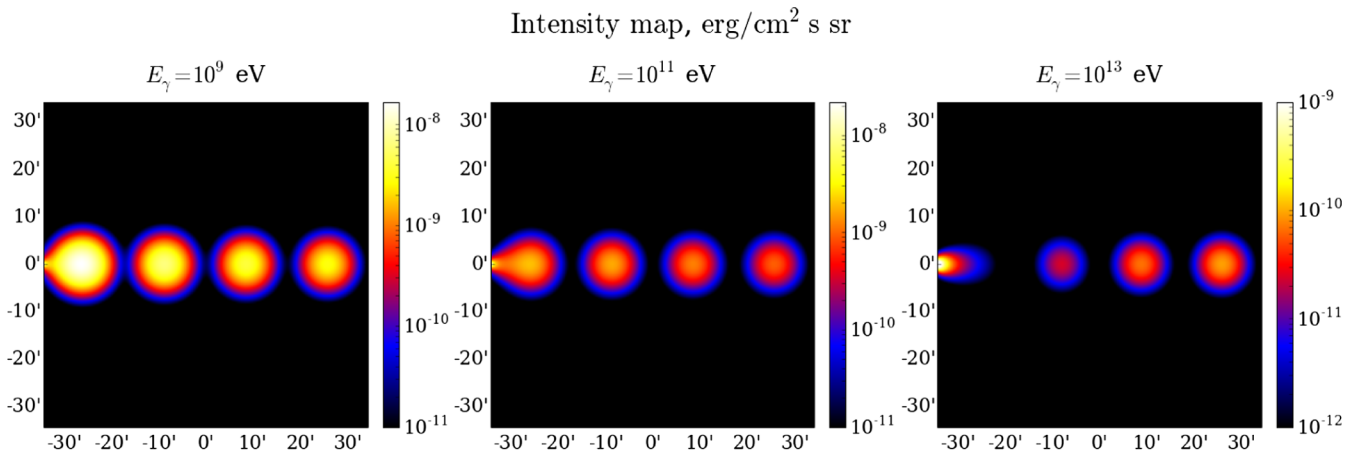


FIG. 7 (color online). The same as in Fig. 6 for the case of a high diffusion coefficient.

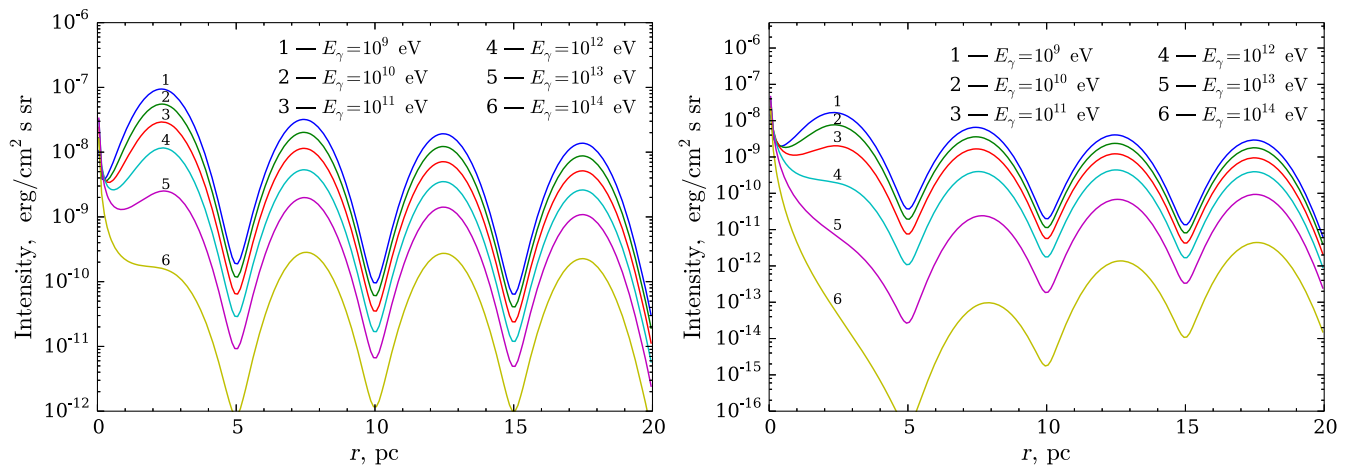


FIG. 8 (color online). The radial intensity profiles for various energies in the case of a group of clouds for a low (left panel) and a high (right panel) diffusion coefficient. The profiles for energies $E = 10^9$, $E = 10^{11}$, and $E = 10^{13} \text{ eV}$ correspond to the intensity maps given in Fig. 6 for the left panel and Fig. 7 for the right panel.

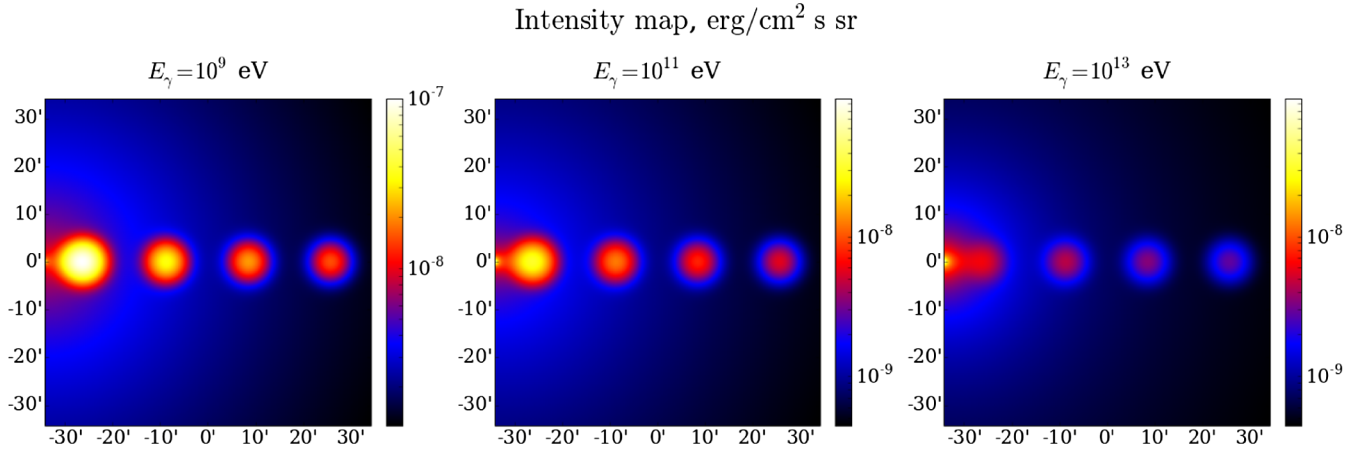


FIG. 9 (color online). The intensity maps of gamma-ray emission from the group of clouds and a homogeneous background at various energies for the case of a low diffusion coefficient. The cosmic-ray source is located at the center of the left side.

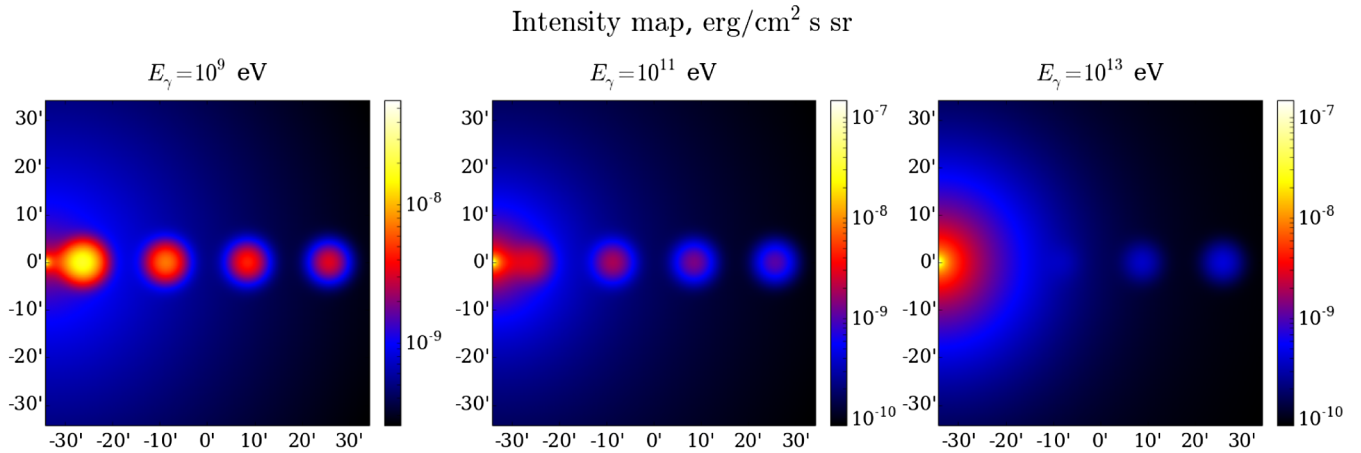


FIG. 10 (color online). The same as in Fig. 9 for the case of a large diffusion coefficient.

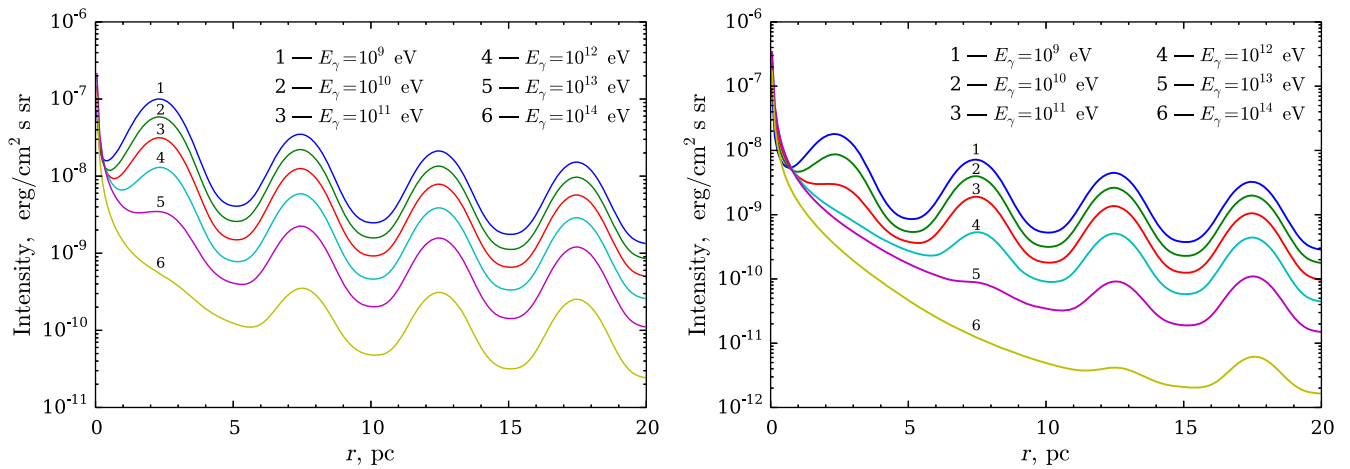


FIG. 11 (color online). The radial intensity profiles for various energies in the case of a group of clouds surrounded by a homogeneous background for the a low (left panel) and a high (right panel) diffusion coefficient. The profiles for energies $E = 10^9$, $E = 10^{11}$, and $E = 10^{13}$ eV correspond to the intensity maps given in Fig. 9 for the left panel and Fig. 10 for the right panel.

TABLE I. Power-law index α for the fit to the gamma-ray intensity profiles for positions of the maximum radiation (the centers of the clouds) shown in the right panel of Fig. 11 (large diffusion coefficient).

E_γ , eV	10^9	10^{10}	10^{11}	10^{12}	10^{13}	10^{14}
α	-0.85	-0.73	-0.49	-0.21	0.53	1.14

relevant curves in the case of no background. The radiation towards the accelerator appears in Fig. 11 because of the presence of the background gas on the line of sight. The results in Fig. 11 show that in the case of fast diffusion the gamma-ray intensity is reduced; at very high energies it disappears from the closest cloud.

To quantitatively describe how fast the gamma-ray intensity decreases with distance, the intensity at the position of the maximum (in the centers of the clouds) shown in Fig. 11 has been fitted with a power law. The calculated power-law indices of the fits for different energies are presented in Table I. It is seen that with an increase of energy the profile becomes flatter. The intensity decreases more slowly in the case of a large diffusion coefficient. Moreover, for the farthest two clouds for energies $E = 10^{13}$ and $E = 10^{14}$ eV the intensity increases with distance. In all cases the intensity at the maximum points changes with distance more slowly than $1/\rho$, where ρ is the projected distance from the source.

The spectral energy distributions of gamma rays in the direction to the centers of clouds are shown in Figs. 12 and 13. The clouds are numbered in the order of their distances

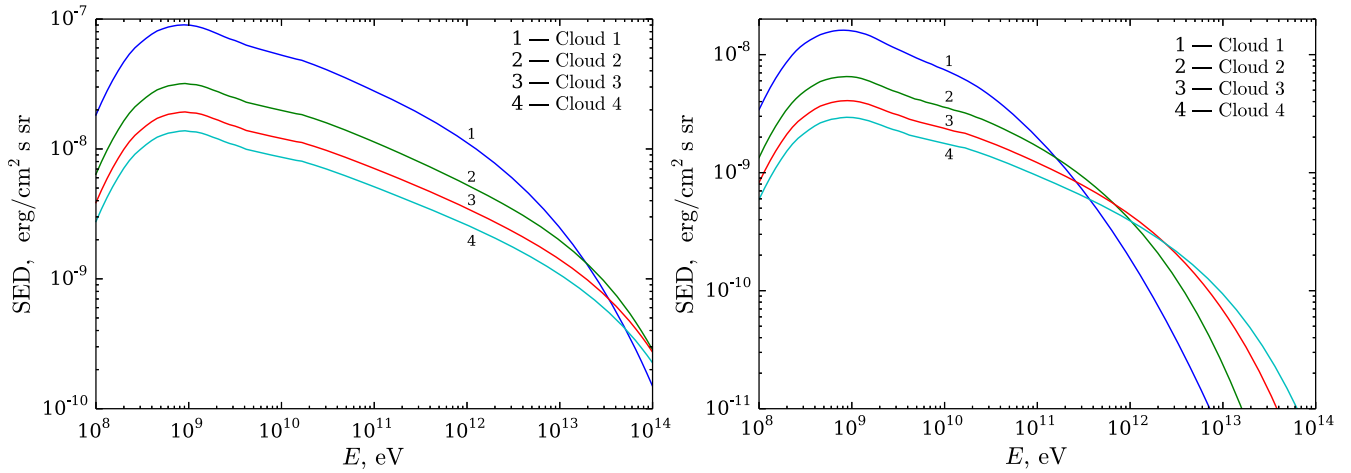


FIG. 12 (color online). Energy spectra of gamma rays in the direction towards the centers of the clouds in the case of no background for a low (left panel) and a high (right panel) diffusion coefficient. The clouds are numbered in order of their distance from the source.

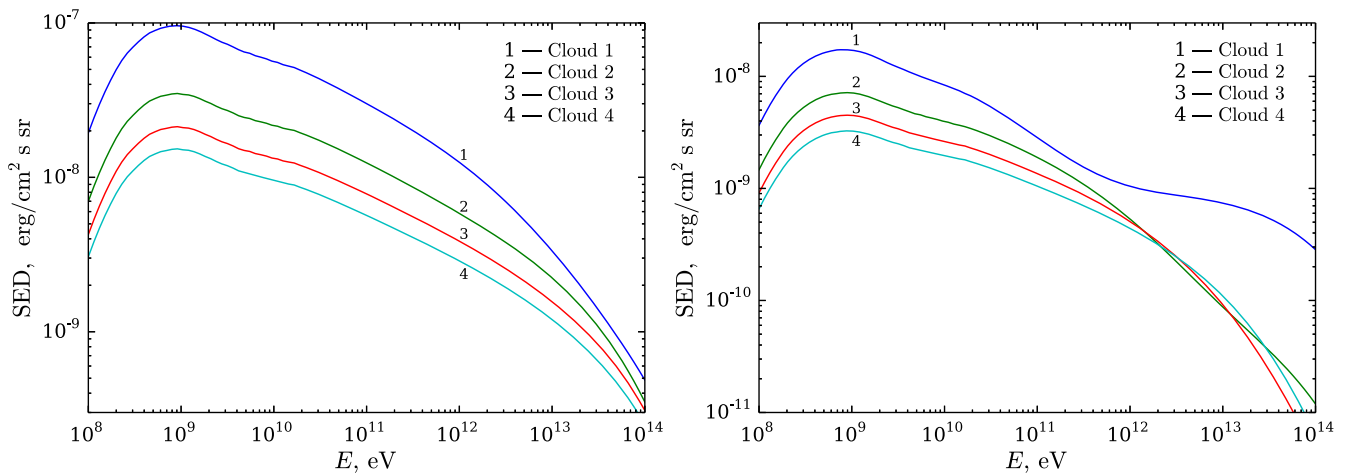


FIG. 13 (color online). Energy spectra of gamma rays in the direction towards the centers of the clouds in the case of the homogeneous background for a low (left panel) and a high (right panel) diffusion coefficient. The clouds are numbered in order of their distance from the source.

to the accelerator. The energy spectra of gamma rays from the clouds are steeper than in the case of the homogeneous cloud surrounding the accelerator (see Fig. 5). Obviously, this is explained by the anisotropic distribution of cosmic rays closer to the accelerator. The picture becomes smoother when clouds are embedded in a homogeneous background gas.

IV. CONCLUSION

One of the major issues in the general problem of the identification of sources of Galactic and extragalactic cosmic rays is the character of their propagation through the turbulent magnetic fields outside the accelerators. Depending on the distance to the source, the level of the magnetic turbulence of the ambient medium, and the energy of particles, their propagation can proceed in the ballistic or in the diffusion regime. While the diffusion of cosmic rays has been comprehensively studied in the literature, the description of propagation in the intermediate stage, i.e., at the transition from the ballistic to the diffusive regime, is a problem of greater complexity in the sense of the exact analytical solutions. To study the dynamics of this transition, we used a simplified approach. Based on the treatment of moments of the Boltzmann equation, we derived a system of equations for the time evolution of the distribution function of cosmic rays. Written in the form of Eq. (11), it describes not only the ballistic and diffusion regimes of propagation as limiting cases, but also the transition stage between these two regimes. This system of equations allows for a simple stationary solution in the form of Eq. (19).

The key feature of this approach is the proper choice of a specific function which describes the pitch-angle isotropization. Within the chosen approach, the isotropization function cannot be strictly determined. Nevertheless, it can be chosen and introduced in a self-consistent manner based on reasonable physics arguments. In this paper, two forms of the isotropization function have been considered: (i) $\phi = e^{-r/\nu}$ and (ii) $\phi = 1/(1 + r/\nu)$. The exponential form seems to be better justified given that in the presence of isotropic turbulence the pitch-angle distribution moments behave exponentially [5]. On the other hand, the form $\phi = 1/(1 + r/\nu)$ provides a simple representation of the stationary solution given by Eq. (23). The results obtained for both forms of the isotropization function are in agreement with an accuracy better than 30%. They also agree well with the integrated Jüttner function proposed in Ref. [4].

The angular, energy, and radial distributions of cosmic rays outside the accelerator, in the general case of their propagation, including the transition stage between the ballistic and diffusion regimes, is described by a surprisingly simple function given by Eq. (34). We should notice that the anisotropy of the cosmic-ray distribution has a strong impact on the gamma-ray morphology. Figure 2 demonstrates that the first moment of the angular distribution of Eq. (29) is very close to the moments given by

Eq. (31) and is obtained from a more physically motivated isotropization function $\phi = e^{-r/\nu}$. This implies that the applied distribution function correctly describes the anisotropy of cosmic rays, and, therefore, provides good accuracy for the calculations of the gamma-ray images.

The anisotropy of the angular distribution of cosmic rays before they enter the diffusion regime of propagation leads to a partial or complete “loss” of secondary gamma rays by the observer. The numerical calculations of secondary gamma rays performed for both the homogeneous and clumpy (consisting of dense clouds) distributions of gas in the vicinity of the accelerator demonstrate the strong impact of the effects of particle propagation in the pre-diffusion regime on the apparent gamma-ray morphology and the energy spectrum. Therefore, the detailed studies of spectral and morphological features of high-energy gamma-ray emission outside the detected (or potential) cosmic-ray accelerators can tell us about the propagation character of cosmic rays after they leave the sites of their acceleration.

ACKNOWLEDGMENTS

We thank the referee for the comments and helpful suggestions. We also appreciate the interesting discussions with Prof. V. Berezhinsky on the importance and different implications of the problem.

APPENDIX: INTENSITY PROFILES

The gamma-ray intensity profile corresponds to the radiation integrated along the line of sight and considered as a function of the projected distance from the source. Let us assume that the angular distribution of cosmic-ray protons is isotropic. In this case the production rate of gamma rays in the direction of the observer is proportional to the density of protons. Since the cosmic-ray density changes according to Eq. (24), the form of the intensity profile is

$$I = \int_{z_1}^{z_2} \left(\frac{1}{r^2} + \frac{c}{rD} \right) dz, \quad (\text{A1})$$

where z axis is directed along the line of sight.

If the region emitting gamma rays is a spherical cloud of radius R with the center at the position of the particle accelerator, then the integration limits $z_{1,2} = \pm\sqrt{R^2 - \rho^2}$ give

$$I_{\text{sph}} = \frac{2}{R} \left(\frac{\arctan \sqrt{\frac{1}{\eta^2} - 1}}{\eta} + X \text{arccosh} \left(\frac{1}{\eta} \right) \right), \quad (\text{A2})$$

where ρ is the projected distance from the source, $\eta = \rho/R$, and $X = Rc/D$. If the emitting region is a strip with width $2R$, and the source of cosmic rays is in the middle of the strip, then the integration limits $z_{1,2} = \pm R$ give

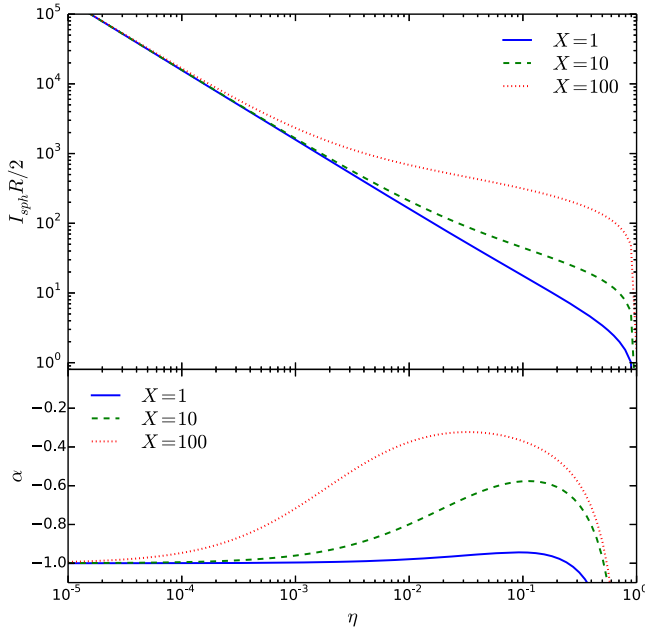


FIG. 14 (color online). The gamma-ray intensity profiles calculated for a spherical homogeneous cloud surrounding the source of protons. The curves correspond to three values of the parameter X . Upper panel: The intensity. Lower panel: The slope of the profile.

$$I_{\text{str}} = \frac{2}{R} \left(\frac{\arctan \frac{1}{\eta}}{\eta} + X \operatorname{arcsinh} \left(\frac{1}{\eta} \right) \right). \quad (\text{A3})$$

The functions $I_{\text{sph}}R/2$ and $I_{\text{str}}R/2$ are presented in Fig. 14 and Fig. 15, respectively. The lower panels show the local slopes of the curves defined as $\alpha = d \ln F(\eta) / d \ln(\eta)$, where $F(\eta) = IR/2$.

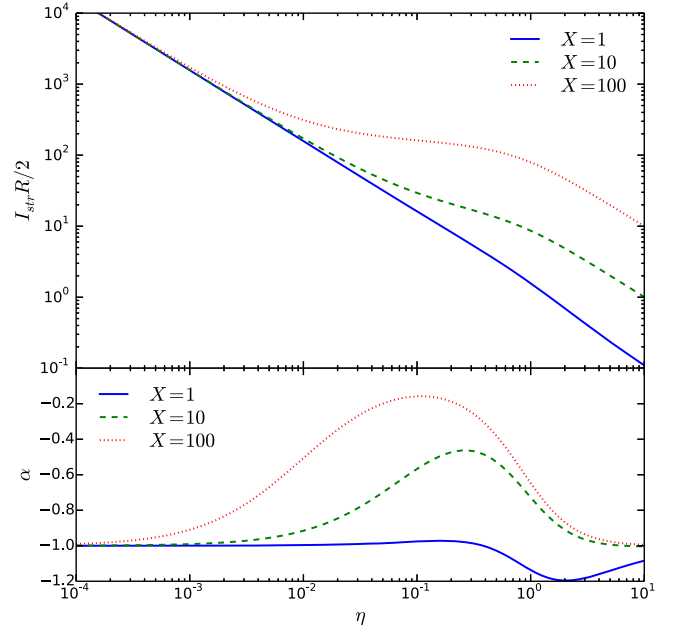


FIG. 15 (color online). The same as in Fig. 14 but for a strip region.

It is seen from Figs. 14 and 15 that at small distances the intensity changes as $1/\rho$. For $X = 1$ this behavior stays approximately the same at all distances. This curve corresponds to the case when the diffusion regime has not been reached at the distance R . Other curves reveal that the transition to the diffusion regime becomes flatter as the distance increases. An integration over a smaller region along the line of sight in the case of a spherical cloud makes the slope of the profile steeper compared to the case of a strip region.

-
- [1] A. Z. Dolginov and I. Toptygin, *Sov. Phys. JETP* **24**, 1195 (1967).
[2] F. A. Aharonian, S. R. Kelner, and A. Y. Prosekin, *Phys. Rev. D* **82**, 043002 (2010).
[3] S. I. Syrovatskii, *Sov. Astron.* **3**, 22 (1959).
[4] R. Aloisio, V. Berezhinsky, and A. Gazizov, *Astrophys. J.* **693**, 1275 (2009).
[5] R. C. Tautz, *Astron. Astrophys.* **558**, A148 (2013).
[6] D. Harari, S. Mollerach, and E. Roulet, *Phys. Rev. D* **89**, 123001 (2014).
[7] R. Aloisio and V. Berezhinsky, *Astrophys. J.* **612**, 900 (2004).
[8] *Nonlinear Cosmic Ray Diffusion Theories*, edited by A. Shalchi (Springer, New York, 2009).
[9] R. Blandford and D. Eichler, *Phys. Rep.* **154**, 1 (1987).
[10] N. Globus, D. Allard, and E. Parizot, *Astron. Astrophys.* **479**, 97 (2008).
[11] S. Gabici, F. A. Aharonian, and S. Casanova, *Mon. Not. R. Astron. Soc.* **396**, 1629 (2009).
[12] F. A. Aharonian and A. M. Atoyan, *Astron. Astrophys.* **309**, 917 (1996).
[13] L. Nava and S. Gabici, *Mon. Not. R. Astron. Soc.* **429**, 1643 (2013).
[14] V. Ptuskin, *J. Phys. Conf. Ser.* **47**, 113 (2006).
[15] E. Kafexhiu, F. Aharonian, A. M. Taylor, and G. S. Vila, *Phys. Rev. D* **90**, 123014 (2014).
[16] S. R. Kelner, F. A. Aharonian, and V. V. Bugayov, *Phys. Rev. D* **74**, 034018 (2006).